Crystal Engineering

International Edition: DOI: 10.1002/anie.201800820
German Edition: DOI: 10.1002/ange.201800820

Reversible Switching between Highly Porous and Nonporous Phases of an Interpenetrated Diamondoid Coordination Network That Exhibits Gate-Opening at Methane Storage Pressures

*Qing-Yuan Yang, Prem Lama, Susan Sen, Matteo Lusi, Kai-Jie Chen, Wen-Yang Gao, Mohana Shivanna, Tony Pham, Nobuhiko Hosono, Shinpei Kusaka, John J. Perry IV, Shengqian Ma, Brian Space, Leonard J. Barbour, Susumu Kitagawa, and Michael J. Zaworotko**

Abstract: *Herein, we report that a new flexible coordination network,* ***NiL₂*** *(L = 4-(4-pyridyl)-biphenyl-4-carboxylic acid), with diamondoid topology switches between non-porous (closed) and several porous (open) phases at specific CO_2 and CH_4 pressures. These phases are manifested by multi-step low-pressure isotherms for CO_2 or a single-step high-pressure isotherm for CH_4. The potential methane working capacity of* ***NiL₂*** *approaches that of compressed natural gas but at much lower pressures. The guest-induced phase transitions of* ***NiL₂*** *were studied by single-crystal XRD, in situ variable pressure powder XRD, synchrotron powder XRD, pressure-gradient differential scanning calorimetry (P-DSC), and molecular modeling. The detailed structural information provides insight into the extreme flexibility of* ***NiL₂****. Specifically, the extended linker ligand,* ***L****, undergoes ligand contortion and interactions between interpenetrated networks or sorbate–sorbent interactions enable the observed switching.*

Crystalline solids are generally regarded as being rigid. However, porous materials such as zeolites[1] and porous coordination networks[2a] can exhibit guest-induced structural transformations when exposed to appropriate stimuli. The degree of flexibility exhibited by such materials can be extreme in porous coordination networks, which are also known as porous coordination polymers (PCPs),[2] metal–organic materials (MOMs),[3] or metal–organic frameworks (MOFs).[4] Flexible microporous materials[5–9] challenge classical sorption classifications because they necessarily change their pore geometry as a consequence of a structural change. For example, whereas type-I (Langmuir) adsorption isotherms (Scheme 1a) are characteristic of rigid microporous materials, flexible microporous materials tend to exhibit "stepped" or "S-shaped" isotherm profiles caused by breathing[6a] or swelling.[6b] When the material becomes porous after activation, the pressure at which the step occurs coincides with a structural transformation between less open and more open phases through a gradual (Scheme 1b, type F-I)[6a] or sudden opening (Scheme 1c, type F-II).[6c] Transformation from a non-porous (closed) activated phase to a porous (open) phase can also occur gradually (Scheme 1d, type F-III) or suddenly (Scheme 1e, type F-IV).[7] Type F-IV

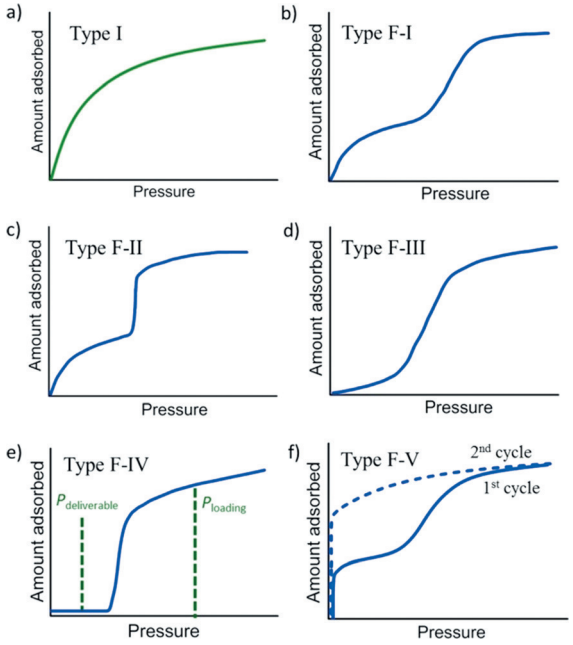

Scheme 1. Proposed classification of isotherm profiles for flexible microporous materials: Type I = rigid microporous material, Type F-I = flexible microporous material (gradual opening from small pore to large pore), Type F-II = flexible microporous material (sudden opening from small pore to larger pore), Type F-III = flexible microporous material (gradual opening from non-porous to porous), and Type F-IV = flexible microporous material (sudden opening from non-porous to porous). Type F-V depicts a shape memory effect[9c,d] and is not relevant for this study.

[*] Dr. Q. Y. Yang, Dr. M. Lusi, Dr. K. J. Chen, M. Shivanna, Dr. J. J. Perry IV, Prof. Dr. M. J. Zaworotko
Department of Chemical Sciences, Bernal Institute, University of Limerick
Limerick (Republic of Ireland)
E-mail: Michael.Zaworotko@ul.ie
Dr. P. Lama, Prof. Dr. L. J. Barbour
Department of Chemistry and Polymer Science, University of Stellenbosch
Matieland 7602 (South Africa)
Dr. S. Sen, Dr. N. Hosono, Dr. S. Kusaka, Prof. Dr. S. Kitagawa
Institute for Integrated Cell-Material Sciences (WPI-iCeMS), Kyoto University Institute for Advanced Study, Kyoto University
Yoshida Ushinomiya-cho, Sakyo-ku, Kyoto 606-8501 (Japan)
Dr. W. Y. Gao, Dr. T. Pham, Prof. Dr. S. Ma, Prof. Dr. B. Space
Department of Chemistry, University of South Florida
4202 East Fowler Avenue, Tampa, FL (USA)
Supporting information and the ORCID identification number(s) for the author(s) of this article can be found under: https://doi.org/10.1002/anie.201800820.

isotherms are desirable for pressure swing gas storage, including adsorbed natural gas (ANG) storage.[7d] This is because type I, F-I, F-II and F-III isotherms (Scheme 1 a–d) retain adsorbed gas at low pressures, thereby reducing working capacity. Unfortunately, whereas there are now circa 100 flexible metal-organic materials, [5b] FMOMS, only 2 FMOMs[7c,d] exhibit F-IV isotherms and high uptake (> 250 cc/cc). Kaskel's group reported $[Ni_2(2,6\text{-ndc})_2(dabco)]$, also termed DUT-8(Ni),[7c] and Co(bdp) (bdp^{2-} = 1,4-benzenedipyrazolate) was reported by Long's group.[7d] The latter is of special interest because it undergoes a structural phase transformation in response to CH_4 pressures between 5–35 atm.[7d] Herein, we introduce a new porous material that exhibits a type F-IV isotherm and high uptake, **NiL_2** (**L** = 4-(4-Pyridyl)-biphenyl-4-carboxylic acid).

A solvothermal reaction of 4-(4-pyridyl)-biphenyl-4-carboxylic acid (**HL**) (Figure 1 a) with $Ni(NO_3)_2{\cdot}6H_2O$ in DMF at 105 °C afforded crystals of the expected[10] diamondoid (**dia**) network **NiL_2**, **X-dia-1-Ni. L** was prepared through serial Suzuki–Miyaura coupling reactions (Supporting Information, Figure S1). Characterization of single crystals of as-synthesized **X-dia-1-Ni**, **X-dia-1-Ni-a1**, by single-crystal XRD (SC-XRD) revealed that it crystallizes in tetragonal space group $I4_1cd$ with $a = b = 24.2018(6)$ Å, $c = 16.2670(8)$ Å, $V = 9528.0(7)$ Å^3. Ni^{2+} cations are coordinated to four oxygen and two nitrogen atoms from four ligands and serve as 4-connected nodes. **X-dia-1-Ni-a1** is a 6-fold interpenetrated **dia** net (Figure 1 c), interpenetration being enabled by adamantanoid cages with Ni···Ni edges of 17.2 Å. The accessible void volume available in **X-dia-1-Ni-a1** is 49 % despite the high level of interpenetration thanks to rectangular channels along the *c* axis (Figure 1 d). The bulk purity of **X-dia-1-Ni-a1** was confirmed by PXRD experiments (Figure 1 f).

X-dia-1-Ni-a1 underwent single-crystal-to-single-crystal (SCSC) transformations after exchange with CH_2Cl_2 or heating at 85 °C for 24 h to less open phases, **X-dia-1-Ni-a2** and **X-dia-1-Ni-a3**, respectively (Supporting Information, Figure S3). Whereas space group and connectivity are unchanged, reductions in cell volume (9528, 8637, and 7441 Å^3 for **a1**–**a3**, respectively), length of the *a* and *b* axis (24.20, 22.17, and 19.95 Å for **a1**–**a3**, respectively) and solvent-accessible void volume (49, 43, and 33 % for **a1**–**a3**, respectively) accompanied the phase changes (Figure 1 e and the Supporting Information, Figure S4). The adamantanoid cages exhibit Ni–Ni–Ni angles of 90°/120°, 80°/126°, and 71°/132° for **a1**–**a3**, respectively. The breathing of the framework is accompanied by changes in N–Ni–N/ C–Ni–C bond angles; 93.0°/101.5°, 90.7°/101.4°, and 88.0°/102.4° for **a1**–**a3**, respectively (Supporting Information, Table S3). **L** also undergoes conformational changes; the dihedral angle formed by the benzoate plane and the pyridine plane is perpendicular in **a1** (89.4°) but parallel in **a2**, (6.1°) and **a3** (1.8°). The breathing

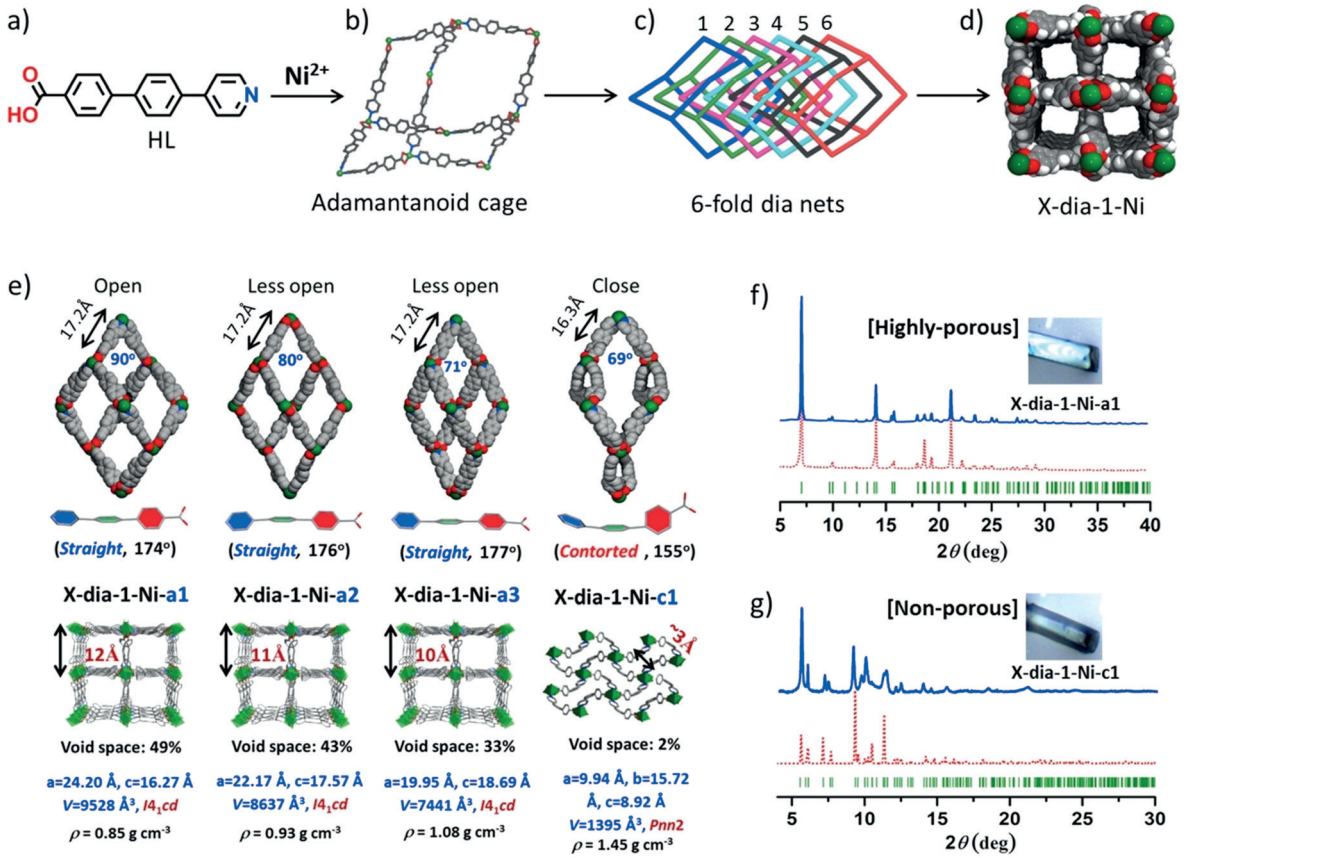

Figure 1. a) Structure of 4-(4-pyridyl)-biphenyl-4-carboxylic acid (**HL**). b) Adamantanoid cage in **NiL_2**. c) 6-fold interpenetrated **dia** nets in **NiL_2**. d) Rectangular channels viewed along the *c*-axis. e) Single crystal structures of the porous (**a1**, **a2**, **a3**) and non-porous (**c1**) phases of **X-dia-1-Ni**. f) Crystal morphology and PXRD pattern of **a1**. g) Crystal morphology and synchrotron PXRD ($\lambda = 0.8262$ Å) pattern of **c1**.[22]

effect can be monitored by powder XRD (PXRD) (Supporting Information, Figure S5); the lowest angle reflection (200) shifts from $2\theta = 7.08°$ in **a1** to $2\theta = 8.94°$ in **a3**.

Heating the **a1**–**a3** phases in vacuo results in a color change from dark green to light green and SCXRD revealed that the light green phase, **X-dia-1-Ni-c1**, is a non-porous **dia** net (orthorhombic space group *Pnn*2). Crystal morphology changes accompany the structural transformation (Figures 1 f,g) as monitored by thermal microscopy. The Ni^{2+} cations of **X-dia-1-Ni-c1** adopt an octahedral coordination geometry and serve as 4-connected nodes as in the open **a1**–**a3** forms. The planarity of **L** as quantified by the N(pyridyl)–phenyl–centroid-C(carboxylate) angle is 174° in **a1**, 176° in **a2**, 177° in **a3** and, remarkably, 155° in **c1** (Figure 1 e). The Ni···Ni edges of the adamantanoid cages decrease from 17.2 Å (**a1**) to 16.3 Å (**c1**). We attribute the existence of **X-dia-1-Ni-c1** to the ability of **L** to contort and changes in the coordination geometry (Table S3). The crystallographic program PLATON[11] revealed that **X-dia-1-Ni-c1** has only 2% solvent-accessible volume. Overall, **X-dia-1-Ni-a1** undergoes a contraction of pore volume from 0.58 $cm^3 g^{-1}$ to 0.01 $cm^3 g^{-1}$ in **X-dia-1-Ni-c1** (Figure 1 e). Such extreme structural transformations between closed and open phases are unusual. We are aware of only four previously reported FMOMs[6b,7c,d,8d] that are known to exhibit such dramatic solvent or gas induced structural change (Supporting Information, Table S4). The purity of the **c1** phase was confirmed by PXRD and synchrotron X-ray powder diffraction (SXRD) experiments. The SXRD pattern of **X-dia-1-Ni-c1** exhibits a diagnostic peak at $2\theta = 5.58°$ ($\lambda = 0.8269$ Å) (Figure 1 g). Thermogravimetric analysis of **X-dia-1-Ni-c1** indicated no weight loss until decomposition at 330 °C (Supporting Information, Figure S6). **X-dia-1-Ni-c1** reverts to **X-dia-1-Ni-a1** when soaked in DMF or toluene at room temperature for 1 min (Supporting Information, Figure S7).

CO_2, with its large quadrupolar moment (13.4×10^{-40} C m^2) and small kinetic diameter (3.3 Å), was chosen to probe how pressure affects switching between the open (**a1–a3**) and closed (**c1**) phases. The low-pressure adsorption isotherm of **X-dia-1-Ni** for CO_2 at 195 K exhibits multiple steps and the surface area of the least-dense phase is 1641 $m^2 g^{-1}$ by Langmuir fitting (Figure 2 a). There is strong hysteresis and clear steps are also present in the desorption isotherm. We conducted in situ PXRD and sorption coincident measurements[12] (Figure 2 b) by placing **X-dia-1-Ni-c1** on a copper plate under high vacuum before collecting PXRD data during CO_2 adsorption and desorption. The diagnostic low angle peak of the **c1** phase (10.03°, $\lambda = 1.54178$ Å) gradually diminished as the diagnostic peaks of **a3** (8.94°) and **a2** (7.93°) appeared, indicative of gate opening (Supporting Information, Figure S8). The steep CO_2 uptake after 0.1 bar is consistent with transformation from **c1** to an open phase. The PXRD pattern did not change markedly in the pressure range 0.2–0.4 bar, which is consistent with the plateau observed in the adsorption isotherm. When CO_2 pressure was increased to 0.42 bar, the diagnostic low angle peak of **a1** (7.08°) appeared. The steep CO_2 uptake around 0.45 bar is consistent with a structural change from **a2** to **a1** that is complete at 0.77 bar. The in situ PXRD patterns on

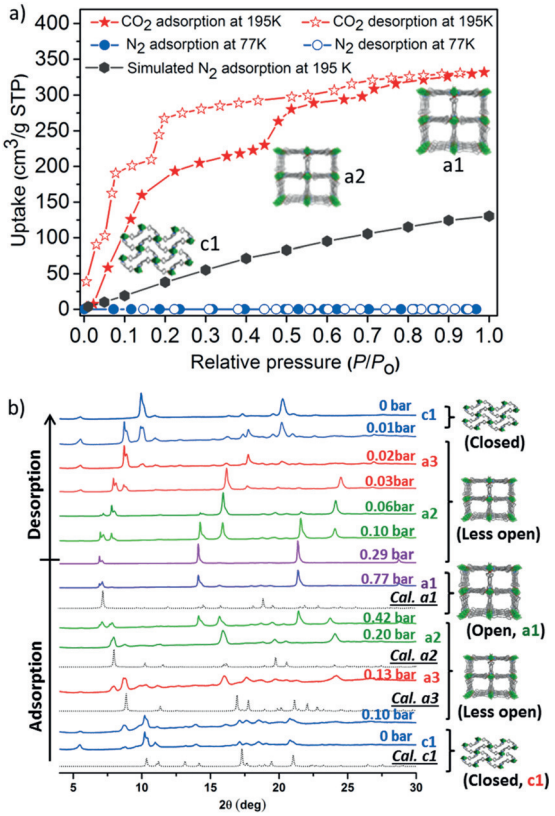

Figure 2. a) Measured CO_2 (195 K) and N_2 (77 K) adsorption isotherms for **X-dia-1-Ni** and simulated N_2 (195 K) adsorption isotherm for **a1**. b) In situ variable pressure PXRD ($\lambda = 1.54178$ Å) of **X-dia-1-Ni** at different CO_2 adsorption/desorption loadings collected at 195 K. Calculated PXRD patterns are black. The PXRD patterns reveal that **X-dia-1-Ni** undergoes structural transformations from **c1** to **a3**, **a2**, and then **a1**. Structural transformations from **a1** to **a2**, **a3** and **c1** occur during desorption.

desorption indicate reversible structural changes between open and closed phases (Supporting Information, Figure S9). **X-dia-1-Ni** exhibited no N_2 uptake at 1 bar and 77 K (Figure 2 a).[13] Simulations predict N_2 adsorption for **a1** (Figure 2 a) and stepwise CO_2 adsorption at 195 K (Supporting Information, Figure S17). The four steps in the 195 K CO_2 sorption isotherm of **X-dia-1-Ni** can be attributed to structural transformations as the framework switches from **c1** to **a3** to **a2** and, finally, to **a1**. That these transformations occur in SCSC fashion enables characterization of each phase in a manner that is atypical of FMOMs, which tend to be poorly crystalline following breathing or swelling.[6b]

Natural gas (NG), is mainly comprised of CH_4 and increasingly utilised for vehicular applications thanks to its geological abundance and low carbon footprint.[14] Current storage technologies typically use cryogenic (liquefied NG at −161 °C, LNG) or high-pressure (compressed NG at 210–250 atm, CNG), conditions that are fraught with hazards and high costs. Adsorbed NG (ANG) using porous materials could mitigate these risks and costs. However, whereas over 20000 physisorbent materials exist (for example, activated carbons,[15a] zeolites,[15b] MOFs,[15c,d] and molecular crystals[15e]), none yet offer a volumetric working capacity that

exceeds 200 v/v as offered by CNG (> 200 atm) at ambient temperature.

A recent computational study of 650 000 porous materials[16] suggests that no current class of rigid physisorbent is likely to exceed the working capacity of CNG. This is mainly because rigid materials typically exhibit type-I adsorption isotherms (Scheme 1 a) and NG remains adsorbed at the typical deliverable pressure of 3–5 atm. Therefore, flexible materials that exhibit type F-IV isotherms as they switch between closed and open phases could achieve high working capacity that has eluded rigid sorbents (Scheme 1 e). However, even before cost and stability issues are addressed, in order to be competitive with CNG, a flexible material must exhibit gate-opening above 5 atm and below storage pressure (for example, 35 or 65 atm). In addition, storage capacity must be greater than 200 v/v at 35 or 65 atm to compete with CNG. Unfortunately, most FMOMs transform between less open (narrow pore) and more open (large pore) phases (Scheme 1 b,c). Indeed, we are aware of only five FMOMs[7b,d,8a–c] that exhibit structure transformations between closed and open phases with appropriate NG gate opening pressure (5–35 atm), and only one exhibits high saturated uptake when open (Table S1).[7d] **NiL_2** is the second FMOM that meets these criteria. CH_4 adsorption isotherms measured at 298 K reveal that **X-dia-1-Ni** adsorbs minimal CH_4 below the phase change pressure (20 bar) and then exhibits an abrupt uptake in adsorption as it switches to an open phase (Figure 3 a). 285 K and 273 K CH_4 isotherms also exhibit a step but with increased uptake before the step (Supporting Information, Figure S21). In situ variable CH_4 pressure PXRD studies were conducted at 298 K by loading activated **X-dia-1-Ni** into a capillary and exposing the sample to methane (Supporting Information, Figure S11). The kinetics of **X-dia-1-Ni** are too slow to observe phase changes; the mixed metal variant (**X-dia-1-$Ni_{0.89}Co_{0.11}$**) more readily shows phase changes under pressure (Supporting Information, Figure S12). **X-dia-1-$Ni_{0.89}Co_{0.11}$** is isomorphous to **X-dia-1-Ni** and was formed under the same conditions. Under vacuum, the **c1** phase of **X-dia-1-$Ni_{0.89}Co_{0.11}$** is present, whereas from 25 bar to 50 bar the peaks of the **a1** phase appear. At 50 bar, **X-dia-1-$Ni_{0.89}Co_{0.11}$** had fully transformed to its **a1** phase. The **a1** phase fully converts to the **c1** phase by around 5 bar. This phase change was also studied by P-DSC.[17] An activated sample of **X-dia-1-Ni** was placed in a DSC sample chamber and exposed to CH_4 in the pressure range 1–50 bar at 298 K. An exothermic peak at 25 bar is consistent with the phase change observed by in situ PXRD. The total CH_4 uptake of **X-dia-1-Ni** at 25 °C is 176 $cm^3 g^{-1}$ (150 $cm^3 cm^{-3}$) for adsorption at 35 bar and 222 $cm^3 g^{-1}$ (189 $cm^3 cm^{-3}$) at 65 bar. The potential working capacity, 147 $cm^3 cm^{-3}$ as calculated from the adsorption isotherm between 35 bar and 5 bar, approaches that of benchmark MOFs (Supporting Information, Table S5). However, hysteresis reduces the working capacity to 110 $cm^3 cm^{-3}$ (5–35 bar) and 149 $cm^3 cm^{-3}$ (5–65 bar), respectively. Approaches to controlling hysteresis are being investigated.

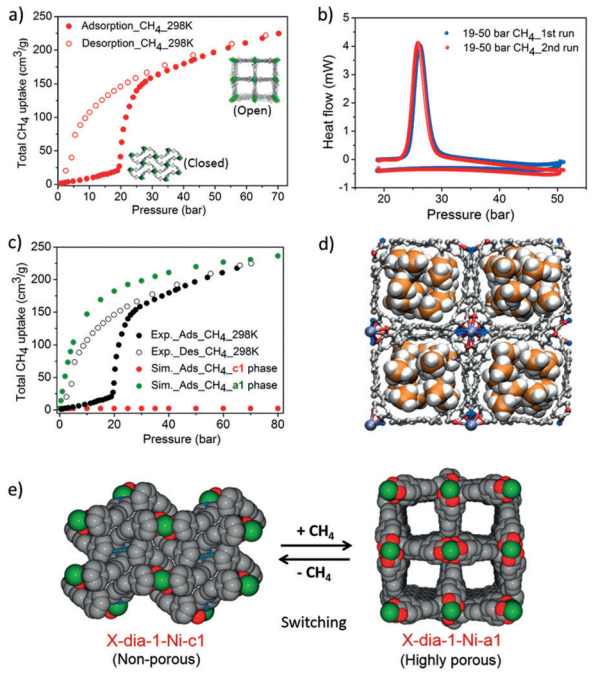

Figure 3. a) Total CH_4 uptake isotherm at 298 K for **X-dia-1-Ni**. b) Pressure-ramped DSC (CH_4, 298 K) for **X-dia-1-Ni**. c) The simulated CH_4 adsorption isotherms in the open (**a1**) and closed (**c1**) phases of **X-dia-1-Ni** at 298 K with the experimental adsorption isotherm. d) The modelled structure at CH_4 saturation in the open phase of **X-dia-1-Ni**. e) Switching between closed (left) and open (right) phases of **X-dia-1-Ni** under CH_4 pressure.

The mechanism of structural flexibility for FMOMs such as paddle-wheel-based pillared-layered frameworks[18] (the prototype for which is DMOF-1[18a]), MIL-53,[5a,6a] and trigonal prism-based networks such as MIL-88,[6b] are based upon hinge motion associated with carboxylate coordination. Structural characterization of the various phases of **NiL_2** indicates a mechanism that largely relies upon ligand contortion. In addition, **c1** is stabilized by interactions between interpenetrated networks. We note that a similar **dia** network formed by a shorter linker ligand, 4-(4-pyridyl) benzoic acid, did not exhibit framework flexibility under the same conditions.[10c] We attribute this to the lesser ability of shorter ligands to undergo extreme contortions of the type observed for **L**. Therefore, the key to the phase changes observed for this prototypal **X-dia** network is the use of the extended "X-ligand", **L**. The single point energies of **L** in **a1** (Figure 4 c) and **c1** (Figure 4 a) were calculated at the MP2/aug-cc-pVDZ level of theory.[19] The energy difference calculated between the two conformations of the ligand is + 165 kJ mol^{-1} (Figure 4 b). Ligands that can contort during structural transformation are rare[20] and no others are yet known to induce framework switching between closed and open phase. Ligand contortion and framework strain might be expected to lead to poor recyclability and reduced performance.[8e] We indeed observed increases in pre-step adsorption at 298 K after four sorption/desorption cycles (Supporting Information, Figure S23 b).

In summary, **X-dia-1-Ni** undergoes pressure- and solvent-induced SCSC transformations between closed and open phases. Four distinct phases of **X-dia-1-Ni** were isolated and studied by SC-XRD, PXRD, and SXRD to provide structural insight into how ligand contortion can enable structural flexibility. **X-dia-1-Ni** is only the second high-surface-area

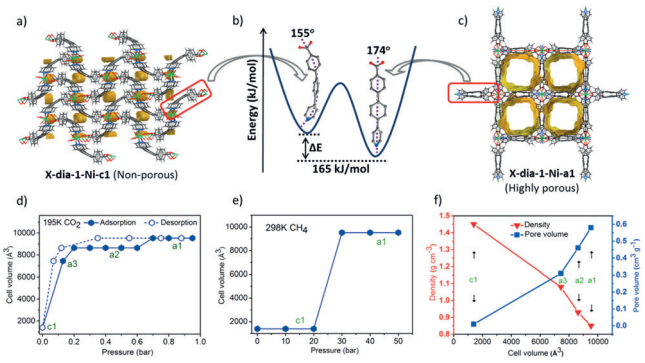

Figure 4. Crystal structures of the a) **c1** and c) **a1** phases of **X-dia-1-Ni**. b) Conformation of **L** in the **c1** and **a1** phases. d) Changes of cell volume of **X-dia-1-Ni** during CO_2 sorption. e) Changes of cell volume of **X-dia-1-Ni** during CH_4 sorption. f) Values of density and pore volume during transformation from **X-dia-1-Ni-c1** to **X-dia-1-Ni-a1**.

FMOM that exhibits CH_4-induced reversible switching with a type F-IV isotherm at pressures relevant for NG storage. Materials such as **X-dia-1-Ni** therefore have the potential to address storage and on-demand delivery of fuel gases by addressing both the working capacity and heat transfer issues that plague rigid sorbents. Perhaps most importantly, **X-dia-1-Ni** belongs to one of the longest studied and broadest classes of MOMs[10a,21] and is therefore likely to be prototypal for a platform of related FMOMs that exhibit switching and type F-IV isotherms, but under different conditions. The possibility of fine-tuning of performance towards a particular gas under a particular set of conditions should be evident from this work.

Acknowledgements

This work was generously supported by Science Foundation Ireland (SFI Award 13/RP/B2549). We thank K. Forrest for the simulations of adsorption isotherms. L.B. thanks the National Research Foundation of South Africa for financial support and P.L. thanks the Claude Leon Foundation for a postdoctoral fellowship. B.S. acknowledges the National Science Foundation (Award No. CHE-1152362), including support from the Major Research Instrumentation Program (Award No. CHE-1531590), the computational resources that were made available by a XSEDE Grant (No. TG-DMR090028), and the use of the services provided by Research Computing at the University of South Florida. N.H. and Su.K. acknowledge the financial support of KAKENHI, Grant-in-Aid for Specially Promoted Research (No. 25000007) from the Japan Society of the Promotion of Science (JSPS). Sh.K. and Su.K. are thankful to the ACCEL program of Japan Science and Technology Agency (JST) for the financial support. We thank Diamond Light Source for access to beamline i11 (EE16167-1).

Conflict of interest

The authors declare no conflict of interest.

Keywords: flexible microporous materials · ligand contortion · methane storage · stepped adsorption isotherm

How to cite: *Angew. Chem. Int. Ed.* **2018**, *57*, 5684–5689
Angew. Chem. **2018**, *130*, 5786–5791

[1] C. A. Fyfe, G. J. Kennedy, C. T. De Schutter, G. T. Kokotailo, *J. Chem. Soc. Chem. Commun.* **1984**, 541–542.
[2] a) S. Kitagawa, R. Kitaura, S.-i. Noro, *Angew. Chem. Int. Ed.* **2004**, *43*, 2334–2375; *Angew. Chem.* **2004**, *116*, 2388–2430; b) S. R. Batten, S. M. Neville, D. R. Turner, *Coordination Polymers: Design, Analysis and Application Introduction*, RSC Publishing, Cambridge, **2009**.
[3] a) T. R. Cook, Y.-R. Zheng, P. J. Stang, *Chem. Rev.* **2013**, *113*, 734–777; b) J. J. Perry IV, J. A. Perman, M. J. Zaworotko, *Chem. Soc. Rev.* **2009**, *38*, 1400–1417.
[4] a) L. R. MacGillivray, *Metal-Organic Frameworks: Design and Application*, Wiley, Hoboken, **2010**; b) D. Farrusseng, *Metal-Organic Frameworks: Applications from Catalysis to Gas Storage*, Wiley-VCH, Weinheim, **2011**; c) H. Furukawa, K. E. Cordova, M. O'Keeffe, O. M. Yaghi, *Science* **2013**, *341*, 1230444.
[5] a) G. Férey, C. Serre, *Chem. Soc. Rev.* **2009**, *38*, 1380–1399; b) A. Schneemann, V. Bon, I. Schwedler, I. Senkovska, S. Kaskel, R. A. Fischer, *Chem. Soc. Rev.* **2014**, *43*, 6062–6096; c) S. Horike, S. Shimomura, S. Kitagawa, *Nat. Chem.* **2009**, *1*, 695–704; d) T. D. Bennett, A. K. Cheetham, A. H. Fuchs, F.-X. Coudert, *Nat. Chem.* **2016**, *9*, 11.
[6] a) C. Serre, F. Millange, C. Thouvenot, M. Noguès, G. Marsolier, D. Louër, G. Férey, *J. Am. Chem. Soc.* **2002**, *124*, 13519–13526; b) C. Serre, C. Mellot-Draznieks, S. Surblé, N. Audebrand, Y. Filinchuk, G. Férey, *Science* **2007**, *315*, 1828–1831; c) A. Kondo, H. Noguchi, L. Carlucci, D. M. Proserpio, G. Ciani, H. Kajiro, T. Ohba, H. Kanoh, K. Kaneko, *J. Am. Chem. Soc.* **2007**, *129*, 12362–12363.
[7] a) D. Li, K. Kaneko, *Chem. Phys. Lett.* **2001**, *335*, 50–56; b) R. Kitaura, K. Seki, G. Akiyama, S. Kitagawa, *Angew. Chem. Int. Ed.* **2003**, *42*, 428–431; *Angew. Chem.* **2003**, *115*, 444–447; c) V. Bon, N. Klein, I. Senkovska, A. Heerwig, J. Getzschmann, D. Wallacher, I. Zizak, M. Brzhezinskaya, U. Mueller, S. Kaskel, *Phys. Chem. Chem. Phys.* **2015**, *17*, 17471–17479; d) J. A. Mason, J. Oktawiec, M. K. Taylor, M. R. Hudson, J. Rodriguez, J. E. Bachman, M. I. Gonzalez, A. Cervellino, A. Guagliardi, C. M. Brown, P. L. Llewellyn, N. Masciocchi, J. R. Long, *Nature* **2015**, *527*, 357–361.
[8] a) H. Noguchi, A. Kondoh, Y. Hattori, H. Kanoh, H. Kajiro, K. Kaneko, *J. Phys. Chem. B* **2005**, *109*, 13851–13853; b) K. Seki, *Phys. Chem. Chem. Phys.* **2002**, *4*, 1968–1971; c) P. L. Llewellyn, P. Horcajada, G. Maurin, T. Devic, N. Rosenbach, S. Bourrelly, C. Serre, D. Vincent, S. Loera-Serna, Y. Filinchuk, G. Férey, *J. Am. Chem. Soc.* **2009**, *131*, 13002–13008; d) Y.-S. Wei, K.-J. Chen, P.-Q. Liao, B.-Y. Zhu, R.-B. Lin, H.-L. Zhou, B.-Y. Wang, W. Xue, J.-P. Zhang, X.-M. Chen, *Chem. Sci.* **2013**, *4*, 1539–1546; e) N. Kavoosi, V. Bon, I. Senkovska, S. Krause, C. Atzori, F. Bonino, J. Pallmann, S. Paasch, E. Brunner, S. Kaskel, *Dalton Trans.* **2017**, *46*, 4685–4695.
[9] a) J. Rabone, Y.-F. Yue, S. Y. Chong, K. C. Stylianou, J. Bacsa, D. Bradshaw, G. R. Darling, N. G. Berry, Y. Z. Khimyak, A. Y. Ganin, P. Wiper, J. B. Claridge, M. J. Rosseinsky, *Science* **2010**, *329*, 1053–1057; b) E. J. Carrington, C. A. McAnally, A. J. Fletcher, S. P. Thompson, M. Warren, L. Brammer, *Nat. Chem.* **2017**, *9*, 882–889; c) M. Shivanna, Q. Y. Yang, A. Bajpai, S. Sen, N. Hosono, S. Kusaka, T. Pham, K. A. Forrest, B. Space, S.

Kitagawa, M. J. Zaworotko, *Sci. Adv.* **2018**, *4*, eaaq1636; d) Y. Sakata, S. Furukawa, M. Kondo, K. Hirai, N. Horike, Y. Takashima, H. Uehara, N. Louvain, M. Meilikhov, T. Tsuruoka, S. Isoda, W. Kosaka, O. Sakata, S. Kitagawa, *Science* **2013**, *339*, 193 – 196.

[10] a) M. J. Zaworotko, *Chem. Soc. Rev.* **1994**, *23*, 283 – 288; b) B. Moulton, M. J. Zaworotko, *Chem. Rev.* **2001**, *101*, 1629 – 1658; c) S. K. Elsaidi, M. H. Mohamed, L. Wojtas, A. Chanthapally, T. Pham, B. Space, J. J. Vittal, M. J. Zaworotko, *J. Am. Chem. Soc.* **2014**, *136*, 5072 – 5077.

[11] A. L. Spek, *J. Appl. Crystallogr.* **2003**, *36*, 7 – 13.

[12] H. Sato, W. Kosaka, R. Matsuda, A. Hori, Y. Hijikata, R. V. Belosludov, S. Sakaki, M. Takata, S. Kitagawa, *Science* **2014**, *343*, 167 – 170.

[13] a) S. Yang, X. Lin, W. Lewis, M. Suyetin, E. Bichoutskaia, J. E. Parker, C. C. Tang, D. R. Allan, P. J. Rizkallah, P. Hubberstey, N. R. Champness, K. Mark Thomas, A. J. Blake, M. Schröder, *Nat. Mater.* **2012**, *11*, 710 – 716; b) Q.-Y. Yang, K.-J. Chen, A. Schoedel, L. Wojtas, J. J. Perry IV, M. J. Zaworotko, *CrystEngComm* **2016**, *18*, 8578 – 8581.

[14] a) J. N. Armor, *J. Energy Chem.* **2013**, *22*, 21 – 26; b) D. Saha, H. A. Grappe, A. Chakraborty, G. Orkoulas, *Chem. Rev.* **2016**, *116*, 11436 – 11499.

[15] a) D. Lozano-Castelló, J. Alcañiz-Monge, M. A. de la Casa-Lillo, D. Cazorla-Amorós, A. Linares-Solano, *Fuel* **2002**, *81*, 1777 – 1803; b) V. C. Menon, S. Komarneni, *J. Porous Mater.* **1998**, *5*, 43 – 58; c) Y. He, W. Zhou, G. Qian, B. Chen, *Chem. Soc. Rev.* **2014**, *43*, 5657 – 5678; d) Y. Peng, V. Krungleviciute, I. Eryazici, J. T. Hupp, O. K. Farha, T. Yildirim, *J. Am. Chem. Soc.* **2013**, *135*, 11887 – 11894; e) A. Pulido, L. Chen, T. Kaczorowski, D. Holden, M. A. Little, S. Y. Chong, B. J. Slater, D. P. McMahon, B. Bonillo, C. J. Stackhouse, A. Stephenson, C. M. Kane, R. Clowes, T. Hasell, A. I. Cooper, G. M. Day, *Nature* **2017**, *543*, 657.

[16] C. M. Simon, J. Kim, D. A. Gomez-Gualdron, J. S. Camp, Y. G. Chung, R. L. Martin, R. Mercado, M. W. Deem, D. Gunter, M. Haranczyk, D. S. Sholl, R. Q. Snurr, B. Smit, *Energy Environ. Sci.* **2015**, *8*, 1190 – 1199.

[17] P. M. Bhatt, E. Batisai, V. J. Smith, L. J. Barbour, *Chem. Commun.* **2016**, *52*, 11374 – 11377.

[18] a) D. N. Dybtsev, H. Chun, K. Kim, *Angew. Chem. Int. Ed.* **2004**, *43*, 5033 – 5036; *Angew. Chem.* **2004**, *116*, 5143 – 5146; b) O. K. Farha, J. T. Hupp, *Acc. Chem. Res.* **2010**, *43*, 1166 – 1175; c) J. Seo, C. Bonneau, R. Matsuda, M. Takata, S. Kitagawa, *J. Am. Chem. Soc.* **2011**, *133*, 9005 – 9013.

[19] H. T. Dunning, Jr., *J. Chem. Phys.* **1989**, *90*, 1007 – 1023.

[20] a) P. Deria, D. A. Gómez-Gualdrón, W. Bury, H. T. Schaef, T. C. Wang, P. K. Thallapally, A. A. Sarjeant, R. Q. Snurr, J. T. Hupp, O. K. Farha, *J. Am. Chem. Soc.* **2015**, *137*, 13183 – 13190; b) S. Krause, V. Bon, I. Senkovska, U. Stoeck, D. Wallacher, D. M. Többens, S. Zander, R. S. Pillai, G. Maurin, F. O.-X. Coudert, S. Kaskel, *Nature* **2016**, *532*, 348 – 352.

[21] B. F. Hoskins, R. Robson, *J. Am. Chem. Soc.* **1990**, *112*, 1546 – 1554.

[22] CCDC 1426847, 1426848, 1426849 and 1426850 contain the supplementary crystallographic data for this paper. These data can be obtained free of charge from The Cambridge Crystallographic Data Centre.

Manuscript received: January 20, 2018
Revised manuscript received: March 15, 2018
Accepted manuscript online: March 25, 2018
Version of record online: April 17, 2018

